Passive Control System For Ease of Weapon Realease From Fighter Aircraft

Ankit Sharma[1], G. Balaji[2]
[1]Dept of Aeronautical
[2]Asst Professor, Dept of Aeronautical
[1, 2] St. Peter's College of Engg. and Technology, Avadi, Chennai,INDIA2

Abstract- *This research work was carried out on simple open cavity at a free stream mach number of 2. The research was conducted to find-out the serration effect to edges of shallow straight cavity and venting to shallow straight cavity. Mean flow and time resolved schlieren visualization and unsteady pressure measurements in the experiment. The ratio of length to depth cavity is 8. Experiments is conducted for straight edge cavities at different Reynolds numbers flow. From these experiment we comes to know that increasing the Reynolds number leads to increases in root mean square pressure inside the cavity. The baseline condition gives that the cavity flow oscillation took place at total 155 m amplitude. The corresponding time history of the pressure on the cavity rear wall and vortex clipping which is responsible for the self-sustained nature of the cavity flow are analyzed. The analysis was carried out among pressure history at points on the rear wall of the cavity and pressure history on the downstream wall of the cavity. Its find out that passive control were identified based on the rear wall Overall Sound Pressure Level (OASPL) and the minimum time lag computed by cross correlation. The venting gives here a good reduction in the cavity oscillations and the rear wall pressure is to reach a steady state value which is preferred in the perception of low cavity noise which leads to reduction in the structural loads and the acoustic loads on electronic components and armament kept near the cavity.*

I. INTRODUCTION

Cavities normally exist in the form of landing gear wheel well and weapon bay in aircrafts. The flow over the cavity tends to produce high magnitudes of oscillation at a frequency that depends on many factors like cavity dimensions, free stream Mach number, boundary layer status at cavity leading edge. A separated shear layer from the leading edge grows and the disturbances is amplified due to Kelvin Helmholtz instability, and the shear layer is wrapped into vortices and the unsteady impingement of the shear layer on rear wall produces pressure waves that travels inside the cavity toward leading edge. The pressure wave energies upon reaching at leading edge and the leading edge completes the feedback loop which leads to self-sustained oscillations. Without control this high amplitude self-sustained oscillations (Up to 160 dB) can damage the sensitive electronic equipment or can affect the weapon release from the air craft. The noise radiated from the cavity need to be controlled. Among passive, open and closed active control techniques, passive control has the advantages over other control techniques in the form of simple, easy to install and maintain. They don't need any external energy input.

Software used for the work

GAMBIT (For grid generation): GAMBIT is a Geometry and Mesh Building Intelligent Toolkit as is one of the main pre-processing tool. Its pre-processor provides concise and powerful set of solid modeling-based geometry tools.

Fluent: ANSYS Fluent is a very powerful and flexible general-purpose computational fluid dynamics software used to flow model, turbulence, heat transfer, and reactions for industrial applications.

Flow field variables to be analysed

- ➢ Mean Pressure
- ➢ Unsteady pressure
- ➢ Oscillation amplitude
- ➢ Velocity Field

II. LITERATURE SURVEY

,**J.E Rosssiter**[1] performed wind tunnel experiment on the flow over rectangular cavity at subsonic and transonic speeds . Navy conducts flight tests at various aircraft attitudes, Mach numbers, and store configurations and determines the initial path taken once the store is released. Modern high performance aircraft carry stores placed inside cavities embedded in the aircraft's fuselage. This implies that during store release phases of operation the aircraft will have to fly with the cavities exposed to the free-stream of air. During this phase, an unsteady, highly energetic flow-field can develop

inside the cavity causing structural, acoustic and aerodynamic problems.

R.L Stalling[2] carry out analysis for store separation from cavity at supersonic speed. The number and duration of flights required can be significantly reduced by predicting trajectories using engineering methods outside of flight test. These predictions are made using store separation analysis, which is a branch of aerodynamics concerned with the trajectories of bombs, missiles and fuel tanks immediately after they are detached from the carriage aircraft.

A.b blair[3] experiment on effect of aerodynamic load of the store separating from cavity. Due to the large loads imparted on the store from the air, these stores do not necessarily move downward. Extreme cases, the store may move up or sideways and impacted the releasing aircraft, potentially causing extensive damage. Store separation analysis can be used to identify these adverse release conditions prior to encountering them during flight tests prevention of this problem lies with extensive pre-flight flow analysis,

F.J Wilcox Jr[4]. experimental measurement of store separation accomplished both in the wind tunnel and through computational fluid dynamics (CFD). Prior to any flight testing, predicted trajectories are obtained using one or both of these methods, and these results are used to determine which configurations require flight tests and to a extent.
The studies have pointed to the shear layer at the boundary of the cavity as the major contributor to adverse separation influences. Passive control of the cavity flow has typically been accomplished through the use of devices such as spoilers and ramps.

D.P Rizzeta[5] researched about ejector mechanisms are used to alleviate the influence of the unsteady and highly three-dimensional aspects of the shear layer. The vorticity of the shear layer and the effects of a passive control can be seen. New aircraft programs, however, are proposing cavities without spoilers or ramps for operational reasons. Store releases must still be predictable and repeatable in order to issue a flight clearance. Therefore, further analysis is required to understand the implications of removing these devices. Extensive wind tunnel research has been accomplished for different trajectories from weapons bays, most notably the Weapons Internal Carriage and Separation (WICS) tests, conducted by the Air Force during the 1990's. Passive control of the cavity flow has typically been accomplished through the use of devices such as spoilers and ramps

Needs of cavity in aircraft

Due to external weapons in the combat aircraft causes higher drag because these weapons are projecting into the flow and also causes higher radar signature. Radar signature is used to identify or distinguish among objects i.e. missiles, aircraft. So, we can make a cavity in the aircraft and we can keep the weapons inside the aircraft i.e. inside the cavity. Generally, this cavity is looks like a groove surface inside the flat surface. It simply looks like a pocket for containing weapons inside so that the drag due to the external weapons are minimized. We can store ad trigger any type of missiles from the combat aircraft

III. METHODOLOGY

I present a methodology that uses in our project on "Bleed system for safe release of weapons from combat aircraft". At the beginning of the chapter, motivation for present methodology is discussed. And some other preliminaries are also added in the next sections. Finally, the main cause of the pressure wave formation is discussed in the last section.

Analysis using ANSYS modeling

The ANSYS Mechanical software suite is trusted by organizations around the world to rapidly solve complex structural and thermal problems with ease.

Structural mechanics solutions from ANSYS provide the ability to simulate every structural aspect of a product, including nonlinear static analysis that provides stresses & deformations, modal analysis that determines vibration characteristics, through to advanced transient nonlinear phenomena involving dynamic effects & complex material behavior.

Kelvin Helmholtz instability

Helmholtz studied the dynamics of two fluids of different densities when a small disturbance, such as a wave, was introduced at the boundary connecting the fluids.

For a continuously varying distribution of density and velocity the dynamics of the KH instability is described by the Taylor–Goldstein equation and its onset is given by the Richardson number Ri. Typically the layer is unstable for R i < 0.25 , Ri< 0.25. These effects are common in cloud layers. The study of this instability is applicable in plasma physics, for example in inertial confinement fusion and the plasma–beryllium interface.

Cavity geometry

The discussion is first restricted on rectangular cutouts. The length of the cavity is Denoted L,D is its depth, and W represents its span wise width

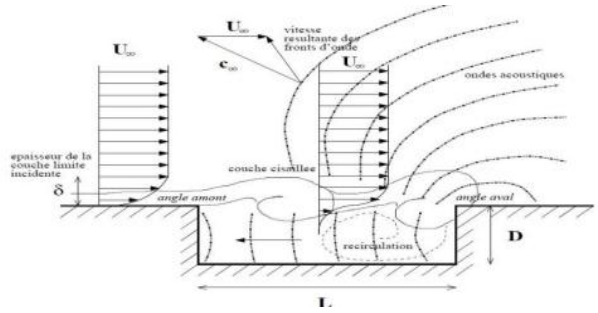

Fig-3

Types of Cavity Flow

The airflow over a cavity will separate from the front edge of the cavity and re- attached downstream, whether the reattachment point is in the cavity itself or downstream at the rear wall will depend on the (l/d) ratio . From this behavior there are three distinct types of flow; they are open, closed and transitional. Cattafesta describes that for an open cavity the shear layer spans the length of the cavity and ultimately reattaches near the trailing edge, where the reattachment region acts as the primary acoustic source. Raman describes a closed cavity to be when the shear layer attaches to the cavity floor then separates in front of the rear wall before reattaching at the trailing edge.

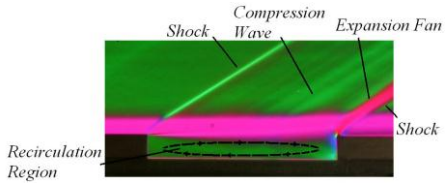

Figure- 4 Schlieren image of a straight edge open cavity, l/d =8

Figure 4 shows a typical open cavity situation wherein the flow separates from the cavity leading edge and bridges the entire length before reattaching at the trailing edge The region beneath the shear layer is the recirculation region where disturbances originating from the trailing edge propagate upstream towards the leading edge. This occurs for all cavities where (l/d) ≤ 9.

The closed flow cavity phenomenon occurs at (l/d) ≥ 12. Figure 5 shows that the flow, after separating from the front edge travels through an expansion fan before reattaching to the floor where it produces a broad region of compression waves.

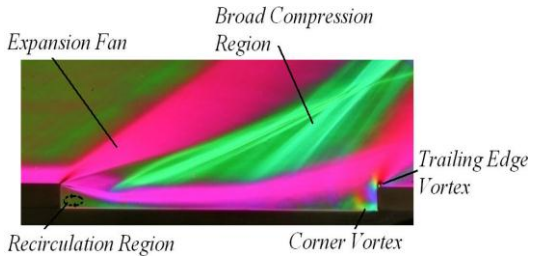

Figure 5. Schlieren image of a straight edge closed cavity, l/d=16

Transitional cavity flow occurs when 9 ≤ (l/d) ≤ 12, and demonstrates similar phenomena to that experienced in closed cavity flow. However, it is less well defined. The shear layer attempts to bridge the gap, but a noticeable downward deflection occurs and either briefly reattaches to the cavity floor or deflects back upto reattach to the rear surface.

3. Oscillatory Behavior

Oscillatory behavior is mainly confined to open cavities and is due to the shear layer impinging on the trailing edge and forcing the flow back toward the leading edge, causing a region of recirculation to occur. The oscillations that result from this phenomenon occur in either the longitudinal, transverse or span-wise directions . However, evidence suggests that the longitudinal oscillations dominate when the (l/d) >> 1. This research is based on cavities with an (l/d) = 8 and will address the issues that occur due to the presence of longitudinal oscillations.

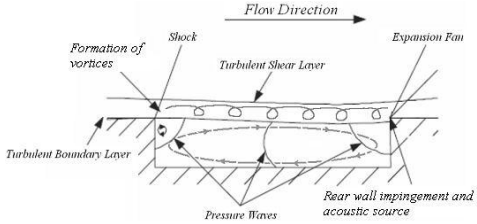

Figure 6. Rossiter acoustic feedback model

In 1964, Rossiter found that the acoustic disturbances are present regardless of whether the boundary layer is laminar or turbulent. This statement is validated by the observation that when the shear layer impinges on the trailing edge, pressure waves propagate back towards the leading edge. They feed the separated shear layer so that a feedback loop is set up generating discrete tones whose frequency is dependent on the velocity, Mach number, (l/d) and the speed of sound in the cavity.

The equation as given is a modified form of the original Rossiter equation as applicable to supersonic cavity

flows. This form of the expression was first given by Heller (1971)and is now widely used.

$$Str = \frac{fl}{U_\infty} = \frac{m - \beta}{\frac{U_\infty}{U_c} + \frac{M}{\sqrt{1 + \frac{\gamma - 1}{2} M^2}}}$$

In the second half of equation 1, m is the mode number, β is the phase delay between impact of the shear layer on the trailing edge and the generation of the acoustic wave, M is the free-stream Mach number, γ is the ratio of specific heats of the fluid and the term Uc/U∞ is the ratio of the convective velocity of the large scale structures in the shear layer to the free stream velocity.

.

Weapon bay aerodynamics

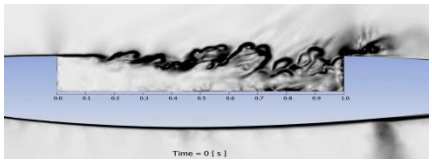

(Fig:7 flow field on the cavity)

Flow control techniques strategies

Following two types are the control techniques;

- **Active control method**

In this type of method generally we use spoilers, blowing techniques etc. by using this we can manage the flow unsteadiness and can control the flow as well. In which the trajectory of the shear layer and diverting it outside the cavity.

- **Cavity shaping**

In his type of methods, we generally use the following methods

- Alteration of incoming boundary
- Slanted walls
- Good performance

Vorticity generation at the leading edge

The conversion of pressure fluctuations, that arrive in the separation region, into vertical fluctuations has been studied by Morkovin and Paranjape. They show how the pressure gradient plays an essential role in the conversion process. Moreover, they suggested that the back-and-forth motion near the separation point helps to convert irrational pressure fluctuations into rotational vorticity perturbations. This mechanism is also clearly illustrated by the linear stability theory of shear flows.

Generation of fluctuations during the impingement

The study of the deformation of vertical structures in the vicinity of the downstream edge is interesting to quantify the equivalent fluctuating force exerted upon the edge and the associated generation of new pressure fluctuations, which in turn will excite the shear layer near the separation point. For thin or turbulent incoming boundary layers, a particular interaction does not dominate; an alter between the different impingement events is rather observed for a long period of time. The random alter, sometimes called jitter, can induce some kind of intermittency, and low-frequency components.
The recirculation zone induced by the cavity walls can modify the trajectory of the vertical structures in the shear layer. This effect is totally ignored in all the theoretical attempts to model the self-sustained oscillations, but can have a non-negligible influence on the variability of the vortex-corner interactions. The details of the vortex-corner interaction determine the instantaneous pressure field, which can drive the shedding of new vortices, as visualized by Tang and Rockwell

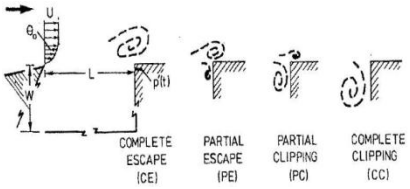

Figure -8: Vortex-corner interactions. From Rockwell and Knisely .

IV. RESULTS ANALYSIS AND DISCUSSION

Supersonic Blow down Wind Tunnel

1. Operational Features

For this research supersonic blow down wind tunnel is used. The test section has cross-sectional area of 155 mm x 90 mm and can produce flow speeds up to Mach 3. The wind tunnel consists of a compressor plant, high pressure reservoir, valve control plus control circuit, stagnation or settling chamber, test section, second throat, subsonic diffuser .The Mach number is a function of area ratio of the throat to the test section cross sectional area and therefore the liners for each Mach number have a different throat area. After the air has passed through the test section it enters a second throat where the air is decelerated and a reduction of the recovery shock on start up occurs. The air then enters the diffuser which further

slows the flow to subsonic speeds and vents it out into the open. The data collection software measures the flow over a four-second period; therefore an adequate duration of steady flow is available for this research.

$$\frac{P_0}{P_\infty} = \left(1 + \frac{\gamma-1}{2} M^2\right)^{\frac{\gamma}{\gamma-1}}$$

The results from using the equation 2 show that the current experiment is running at a Mach number of 2.0 ± 0.1, the calculations can be found in appendix D.

Experimental Set up

A sample of data was taken from the two transducers and the thermocouple over a period of 30 seconds, in which time the wind tunnel would start up, overshoot, undershoot and eventually reach the steady flow condition. This data is sampled at a 400 Hz rate for 12000 samples.

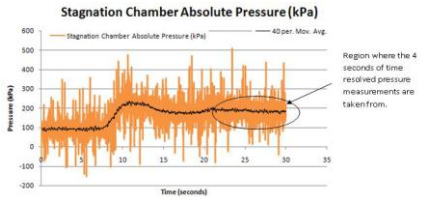

Figure 9. Pressure history for the stagnation chamber on start up of the wind tunnel

Figure- 9 shows the output from the stagnation chamber transducer when run at 200 kPa. It shows the pressure building on start up then it overshoots the required value before dropping below and then finally flattening off to produce a steady signal.

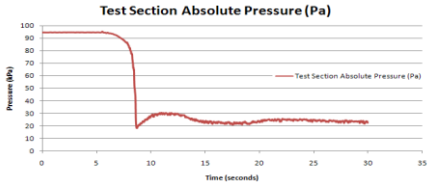

Figure -10. Pressure history for the test section on start up of the wind tunnel.

Figure-10 show the output of the molecule test section molecule. The above plot shows that on start up the test section pressure drops; this is due to the reduction in pressure as the flow is accelerated. However, the total pressure value will stay the same.

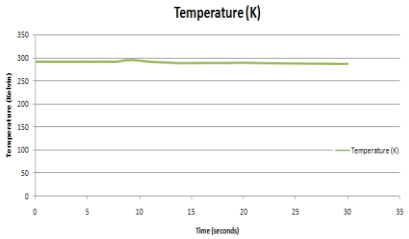

Figure -11 Temperature history for the stagnation chamber on start up of the wind tunnel

Figurer-11 shows the temperature history for the 30 second period. Here the plot shows is that there is a slight increase in the temperature inside the stagnation chamber on start up but then it evens out. It can be noticed that there is a slight drop off of the temperature toward the end of the sample time; this is due to the continual expansion of air. The temperature drop is only temporary and due to the time delay between runs, when the reservoir is refilling, the stagnation chamber temperature returns to its original temperature.

Experimental Cavity Model In Case of Serrated Edge

1. Specifications

The model used in this report is the model that was designed and used by Sally J Moon in 2008. This model so that it could be used with serrated leading or trailing edges. It allows inserts with serrated edges of 60 and 120 degrees to beinserted in the leading or trailing edge with an opposite straight edge. Fig-12 (a)

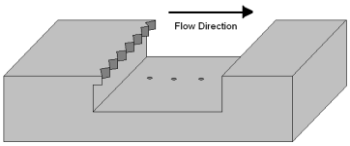

Figure -12 (a) shows the serrations as they appear on the leading edge of the model. For both serration angles the cavity can be configured for either serrations on the leading or trailing edge with an (l/d) = 8.

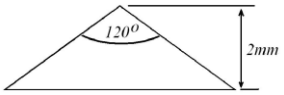

(b) Figure -12 (b) shows the geometry of the 120 degree serrations that will be used in the cavity.

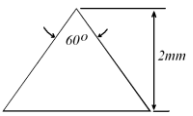

(c) fig -12 (c) shows the geometry for the 60 degree serrations that will be used on the cavity.

The location and exact position of the serrations will be discussed in more detail in subsequent sections.

2. Theory behind Serrations

Serrated edges are not an entirely a new concept. Schwind and Allen (1973) used serrations on the leading edge of a NACA 63-009 airfoil in an attempt to reduce the P_{rms} at leading edge. This experiment research was particular based on fact that owls fly silently since they have fine serrations on the leading edge of the first two feathers .

Hersh in 1974from experiment got that by adding serrations to the leading edge of either stationary or rotary airfoils they could successfully reduce the overall sound pressure level. One more latest research into the effect of serrations was conducted by Yan in 2007. In that paper they were investigating the effect to the nozzles of high bypass ratio turbofans of adding serrated edges. The result they got on reduction of the turbulent kinetic energy levels could be a mechanism which leads to reduction in sound level . Their experiment out comes gives that by choosing correct dimensional configuration of the serration reduction in noise can be achieved.

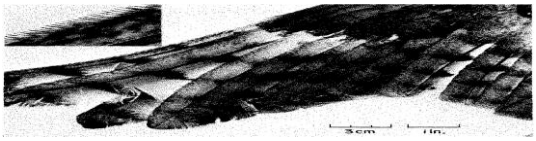

Figure-13

Equipment, Data Collection and Analysis

A. Pressure Transducers

1. Equipment

Kulite miniature pressure transducers were used in this series of experiments to gather time resolved unsteady pressure measurements from the cavity floor. They are located in the centre of the cavity width and along the cavity length at the location indicated in fig 14, where the numbers indicate the location of each transducer.

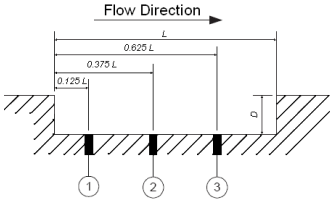

The location has been chosen so that the pressure readings are not affected by pressure changes as a result of the side wall effects. Therefore, the time-resolved unsteady pressure measurements are treated as 2-dimensional flow readings.

2. Data collection

The experiments in this research use a constant free stream Mach number of 2.0 ± 0.1. Tests were conducted using the straight edge cavity at four different Reynolds numbers. Further tests were conducted at a single Reynolds number with serrations being added either to the leading edge or the trailing edge, but not both at the same time.

Kulite pressure transducers connected to interface BNC2090 which gathers the data and sends it to the computer.

According to Nyquist sampling theorem the signal can be re-constructed as long as it is being sampled at twice the highest known frequency. Therefore, 1 MHz should suffice.

3. Analysis

The data that was collected during each wind tunnel run was processed using the Matlab code . This code converts the transducer signal into pressure and by means of a fast Fourier transformation (FFT), determines the frequency spectrum of the signal. The first plot to be analysed is the spectrogram. This allows for the analysis of the frequency output of the signal over time. It determines whether the signal is changing significantly over time or if the same frequencies are present over the sample time period.

Then a second analysis was conducted to find which frequencies are dominant and the SPL that arise from each frequency packet. The information will also be used to find Root Mean Square pressure values within the cavity and see how these values changes with Reynolds number. The full analysis is described in section four.

B. Pressure Sensitive Paint and the Wind Tunnel Top Window

1. Equipment

The major advantage of PSP is its ability to gather a large amount of surface pressure data of any object for relatively low cost and set-up time. This meant that the model was very complex and required many hours spent in designing and fabricating the model, and once it had been built the data

gathered was still not sufficient to accurately map the pressure distribution over the entire surface.

Pressure sensitive paint exploit the sensitivity of some of molecule to O_2 and how their luminescence is reserved by the O_2. During excitation from a Ultra Violet lamp a glowing molecule absorb the photon and jumps to an higher level energy state. How much oxygen is present will determine how much the molecule will illuminate. After being excited the molecule then comes back down to lower ground state, on the way emitting a photon of a certain wavelength. The wavelength of the emitted photon is in the red region of the colour spectrum, therefore, a red filter is used along with a very high speed picturing camera to detect the emitted photon and record the change in luminescence.

The Stern-Volmer equation is used to quantify this information, shown here as equation.

$$\frac{I_{ref}}{I} = A + B\left(\frac{P}{P_{ref}}\right)$$

Figure 15 is a graphic representation of the components of the PSP; these include a thin

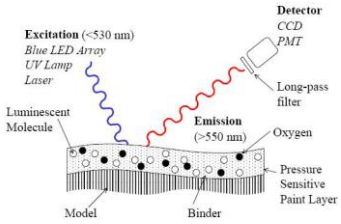

Figure 15. Components of a PSP system

Polymer layer embed with molecule luminophore . The O_2 from the flow interacts alongwith the polymeric layer and its concentration with in the layer is directly proportional to the static air pressure on the upper surface. A UV light source excite the luminescent molecules, and the output is a function of the oxygen concentration. The sensor then detects the light that is emitted from the molecules and is able to present this as a picture with different regions of luminescence.

One major disadvantage of PSP's is that they are temperature sensitive, and therefore this must be taken into account.

2. Data Collection

One of the objectives of this research was to use pressure sensitive paint in conjunction with the time resolved unsteady pressure transducers. However, to successfully acquire data that can be compared to the unsteady pressure measurements the PSP must have a response time of less than 1ms. During this research PSP tests were conducted to quantify the response time of the paint. The shock tube was used as it is able to provide a pressure step, the images below in fig 16 show the shock wave passing in front of a painted test strip

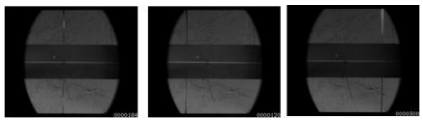

Figure 16. Shock wave produced by the shock tube.

Directly behind the shock is a region of high pressure, this high pressure according to equation 5 will be seen as a drop in luminescence of the paint. Therefore, the time it takes for the paint to respond to this change in pressure, will be the response time of the paint. From this information it can then be determined whether the PSP is suitable to be used to gather unsteady pressure data. In figure the test strip shows two different paints separated by a white strip. The images in figure were taken without using the UV lamp or red filter and hence they do not show the change in luminescence.

3. Analysis

In order to analyse the data that is collected a Matlab program is used to detect the change in luminosity of the paint. Another student, Olivier Picolet, conducted the analysis that is shown below, due to delays with availability of the camera this student will be implementing the findings from the experiment that was conducted for the current project.

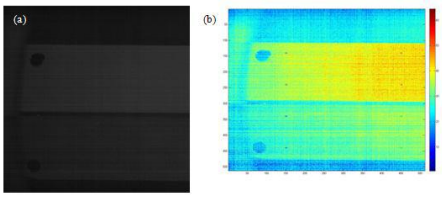

Figure 17. (a) Image from Redlake camera. (b) Matlab version of image

The four ovals in fig 17 (b) show the locations of a strip one pixel in width where the luminosity data was taken from. The resolution of this image is quite poor due to the high level of noise that comes from the camera. As previously mentioned the test strip is required to be illuminated by a UV lamp and a red filter is fitted to the camera.

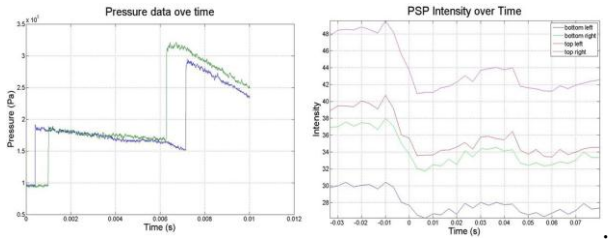

Figure 18. (a) Pressure history recorded from pressure transducers inside shock tube. (b) PSP intensity during change in pressure.

Time zero in fig 18 (b) is when the shock passes over the test section, due to the low frame rate (300 fps) the response time is very difficult to estimate. However, what we are able to see is that both paints have responded to the increase in pressure, and have decreased in luminosity. Figure 18 (a) is the pressure history taken upstream from the test section, note here the time scale to the two plots are different.

C. Schlieren Visualisation

1. Equipment

The schlieren technique has the ability to gather several types of data measurements simultaneously. It takes advantage of the fact that varying density within a fluid leads to a refractive index gradient. The associated light deflections allow otherwise invisible phenomena to be observed. These phenomena include compression fans, vortices, expansion, shock waves and boundary layers. This can be explained by the following equation:

$$\frac{c_0}{c} = n = 1 + K\rho$$

This equation shows that the refractive index is a function of the density of the medium. Therefore light travelling through a region of greater density will move more slowly and the associated light wave front will be deflected towards the region of higher density. The basic principle of the schlieren technique is to separate the un-deflected and deflected light beams, by jamming out deflected beams so they don't appear on the screen recording.

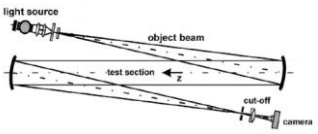

Figure 19. Set up of z-type schlieren system

Figure 19 shows a typical z-type schlieren system which consists of a light source, a slit or pin hole to define the shape of the light source, two lenses or spherical mirrors, a knife edge or colored filter and a screen or camera to capture the image. In the current project a point light source is passed through the slit or pin hole, then through the color filter before it is reflected by spherical mirror transforming it into a beam of parallel light which is then passed throughout the test section. The second mirror then focuses the light beam through the colored filter or knife edge and onto a screen. The image produced by this process records the changes in density as a change in color or hue.

2. Data Collection

The still images in colour were taken with an exposure time of 200 μs and six photos were taken over the four second run duration. These images were taken using a digital camera. After being downloaded from the camera they could be directly analysed from the computer screen.

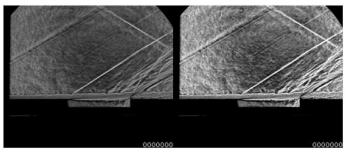

Figure 19. (a) Before auto-correction. (b) After auto-correction.(b)

The time resolved images were captured with exposure time of 1μs. The images that were produced were then enhanced using an autocorrect function in Microsoft Office Picture Manager, which allows the detail in the pictures to be seen more clearly.

3. Analysis

The colour images, which have been presented in previous sections, clearly identify the flow features that were discussed in the first section. Time resolved images have not previously been taken of cavity flows at frame rates of 250,000 fps. Therefore, the features within the time resolved images have been able to shed light on previously unseen phenomena. A full analysis of the schlieren images is presented in section four.

RESULTS AND DISCUSSION

The results presented below extend previous research of the flow over straight cavities mentioned earlier sections. The combination of single image color schlieren visualization, time resolved monochrome schlieren visualization and measurements of unsteady pressure has allowed flow inside the cavities to be investigated with greater clarity. The

unsteady pressure data can be compared to the high speed visualizations, which helps to better describe flow behavior.
This section outlines the analysis conducted in two major categories: The flow over straight cavities at different Reynolds numbers and the effect of adding serrated edges or vent to the cavity

B. Straight Edge Cavity (l/d=8)

1. Schlieren Visualisation

The first series of experiments focused on straight edge cavities. Direction indicating colour schlieren photographs were taken to observe the flow patterns within the cavity. This allowed one to confirm the existence of these patterns predicted by theory, before the inclusion of serrations.

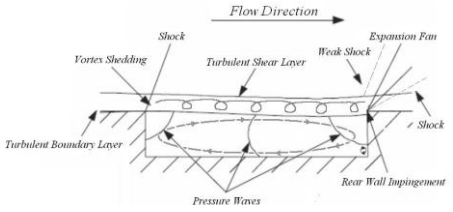

. Figure 20 shows a schematic of the leading edge shock is caused by the lifting of shear layer and is observed as a faint green line in fig 20 that commences at cavity leading edge. The next flow feature is the turbulent shear layer, which impinges on the rear wall and causes pressure waves to be reflected back into the cavity. The turbulent shear layer is clearly seen . A measure of the turbulence of the shear layer is the number and distribution of the compression wavelets that are present downstream of the cavity leading edge. At the trailing edge is the expansion fan which is preceded and then followed by a shock wave. The first shock and then expansion fan at the trailing edge is a result of the flow spilling out of the cavity. Inside the cavity it is reasonable to expect the presence of a recirculation region. However, Reim point out that the waves oscillating with in cavity are basically transient strong acoustic waves and hence can only be visualized in a time resolved visualization.

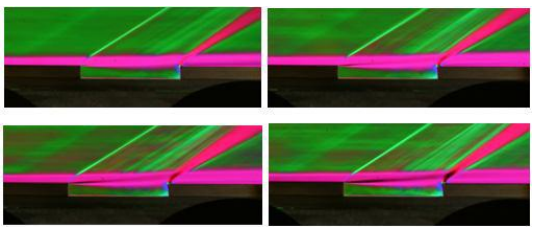

Figure 21. (a) Rex = 4.6 x 10^6. (b) Rex= 7 x 10^6. (c) Rex = 9.8 x 10^6. (d) Rex = 12 x 10^6

In figure 21 the above flow features are very clearly seen and as mentioned above there is the presence of a light green region. These show compression wavelets, which are formed due to high turbulent shear layer. This can be most clearly seen in fig 21 (c) and (d) where the large scale structures are forming a jiggered surface. These compression wavelets become more important as the Reynolds number increases.

It is important to observe that as Reynolds number increases because the density is increased. The sensitivity of schlieren images depends also on the mean density level, and hence flow structures may become more prominently displayed if the density is increased. The same features may exist in similar form at lower density levels; however, they may not be as clearly visible. The boundary layer is noticeable in these images as the pink region up to the cavity leading edge. The thickness of the boundary layer can be calculated using an equation proposed by Crocco and Lees The expression of Crocco and Lees is given by:

$$\frac{\delta_b}{x} = \frac{0.037}{(Re_x)^{\frac{1}{5}}} \frac{C_{f_M}}{C_{f_i}} \frac{1}{(\delta^{**}/\delta)}$$

Here x is length of the plate up to the leading edge of cavity which in the present case is 184 mm. δb is the thickness of the boundary layer at leading edge of the cavity (before it separates and forms the shear layer). C_{fM}/C_{fi} is the compressibility correction and δ** is the momentum thickness, with the ratio δ**/δ being evaluated by assuming a 1/7th power velocity distribution.

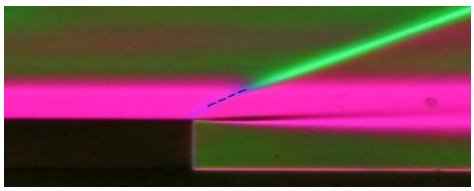

Figure 22. Magnified view of leading edge shock.

The magnification of the schlieren images at the cavity leading edge, fig 22, shows how the Mach number in boundary layer change as the surrounded shock wave changes in inclination before disappearing after reaching the subsonic region. A magnified image of the leading edge shock; here it can be observed that the shock angle changes throughout the boundary layer. The images are for Reynolds number, Rex, of 4.6 x 10^6. The Mach number for the free-stream flow is confirmed to be 2.1. The Mach number for flow in upper section of boundary layer is 1.72, and the Mach number in the mid region of the boundary layer is 1.27

The analysis also conducted for the case with a Reynolds number of 12 x 10^6. The free-stream Mach number was calculated to be 2.27, when compared to the result from equation 2 it is within 15%. The Mach number that was found for different locations within the boundary/shear layer is consistent with the values calculated at the lower Reynolds number, which indicates that the increase in density does not affect the Mach number within the boundary layer.

2. High Speed camera data

The used shadowgraph system to visualise the flow field and take instantaneous images of the cavity flow. They did this at a frequency of 1,000 Hz, with exposure times of less than 4μs. In the current experiment, with the assistance of Dr Harald Kleine, a system was set up to take images at 250,000 frames per second with an spotlight time of 1 μs.

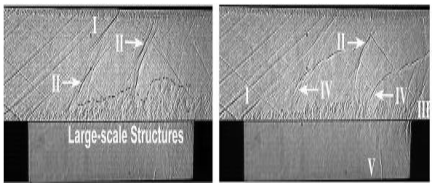

Figure 23. Instantaneous shadowgraph images (a) Type I and type II waves and large scale structures. (b) Type I, II, III, IV and V waves.

Figure 23 shows the waves that were identified by Zhuang et al. In the current project we are able to clearly see the formation of these waves and also track how they change over time. All wave types including type V are clearly visible in fig 23. For the full series of images refer to Appendix O.

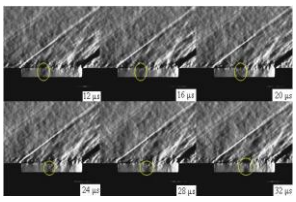

Figure 24. Time resolved schlieren images.

Figure 24 shows the pressure wave propagation. All 102 images can be found in appendix O. From analysis of the pictures shown in figure 23 it comes that the pressure wave move in an average of 1.2mm between the frames, imparting it speed of 300 m/s. Assuming the wave propagates back and forth within the cavity, we can also assume that the wavelength of the flow is 2L = 64mm. Then using the equation:

$$f = \frac{v}{\lambda}$$

3. Unsteady Pressure Measurements

The unsteady pressure measurements were taken at the Reynolds numbers mentioned above; firstly for the single cavity geometry, the results for Reynolds number of 7.2 x 106 will be used as a comparison for the addition of serrations. The oscillations inside the cavity occur in the longitudinal, span-wise and transverse directions. It is known that the longitudinal mechanism dominates in cavities with (l/d) ≥ 2.

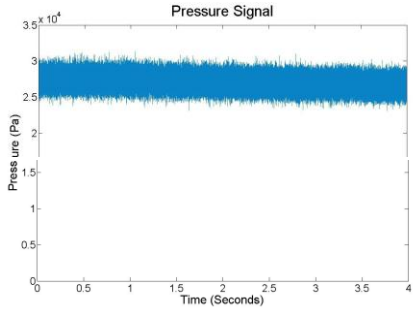

Figure 25. Typical the unsteady pressure signal over a four second time period.

Figure 25 is a schematic breakdown of the FFT process. Effectively the FFT breaks the signal into the individual frequencies and then plots each frequency against the output. As mentioned in previous sections, to conduct the FFT correctly the data must be sampled at least twice the frequency of the most important frequency. The power under the signal is conserved during the process. The data that is output can then be presented as the SPL.

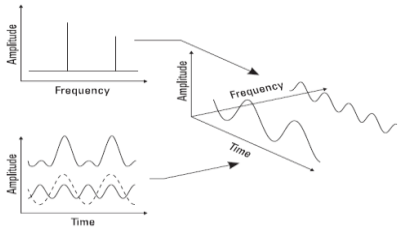

Figure 26. Breakdown of the fast Fourier transform

The reference pressure that is used threshold of hearing level pressure, Pr = 20 μPa. The SPL is given in dB and is generally given by:

$$SPL = 20\log_{10}\left(\frac{\sqrt{P'^2}}{P_r}\right)$$

This allows for the SPL to be visualised across the entire frequency spectrum. Initial research into the frequencies present in the signal were conducted to find how the frequency spectra changed over time. The spectrogram function in Matlab was used to gather this data. The sampling frequency

used to obtain the spectrogram was 1 MHz, which allows frequencies up to 500 kHz to be observed.

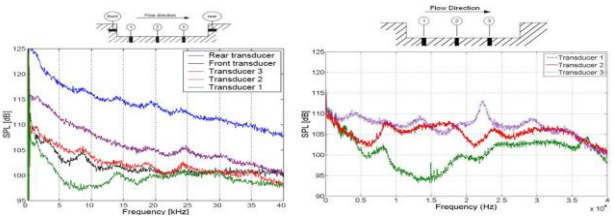

Figure 27. (a) Open straight cavity results. (b) Present Open straight cavity results.

Figure 28 plots the output of transducer 3 and overlaid on top are the Rossiter modes. Here we can see the existence of discrete resonant frequencies. The peaks are quite weak, which attribute to the high Mach number and shear layer thickness. He mentions that the thicker shear layers tend to smoothen the gradient in flow. The rear most transducer shows the presence of the highest frequency due to the close proximity to the impinging shear layer. The frequency that is present at 23 kHz is the most prominent frequency and the only frequency peak that does not correlate with the Rossiter modes. This is most likely a result of some low frequency vibrations that are either inherent in the data acquisition system or vibration due to the impingement region inside the cavity.

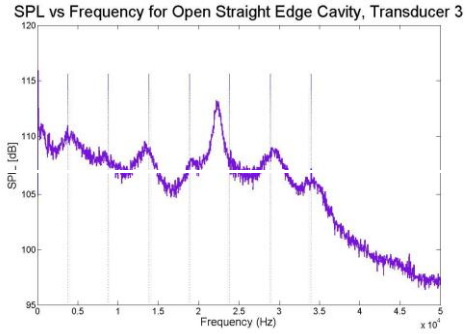

Figure 28. Open cavity Sound pressure level spectrum for transducer 3. Rex = 7 x 10^6

Figure 29 shows a linear association among the root mean square pressure value and the Reynolds number. This means physically that at higher altitudes the cavity flow properties may be less dominant. Therefore, for a supersonic aircraft flying at altitude the noise and vibrations would be less noticeable than when they are flying near ground level.

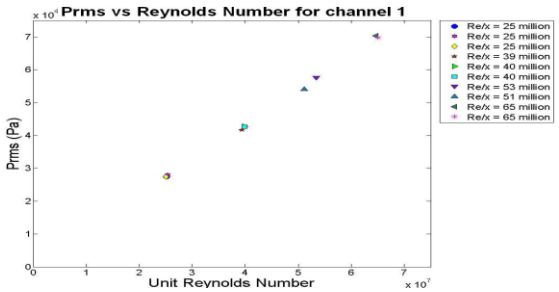

Figure 29. Changing Reynolds number for channel 1 Against Root mean square pressure plotted

C. Serrated Edge Cavities (l/d=8)

1. Schlieren Visualisation

Schlieren visualisation was used to compare the effects of adding serrations to the cavity. As previously mentioned it is expected that the addition of serrated [edges] will alter the strength of the leading edge shock and also create streamwise vortices that might mitigate effects of strong span-wise vortice of the big scale structures in separating shear layer.

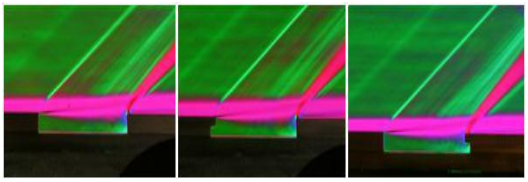

Figure 30. Rex = 7 x 10^6. (a) Straight edge cavity. (b) 60^0 leading edge serrations. (c) 60^0 trailing edge serrations.

Figures 30 (a), (b) and (c) were all taken as a Reynolds number of 7 x 10^6 and compare the straight edge cavity situation, fig 31 (a), to the cavities that have serrated edges, figs 30 (b) and (c). The presence of compression wavelets is less prominent in the figure with leading edge serrations as compared to the straight edge situation, whereas in the third figure the compression waves seem to be more prominent. This leads one to believe that the serrated rear edge is actually feeding the shear layer and inducing turbulence. Therefore, one would expect that further research into the sound pressure levels will show an increase in SPL when 60 degree serrations are added to the trailing edge.

Figures 31 (a), (b) and (c) compare the addition of 120^0 serration to the cavity and were also taken at a Reynolds number of 7 x 10^6. The condition with 120^0 leading edge serrations show a weak leading edge shock wave; which is due to dispersal of the shock wave over the protruding serrations.

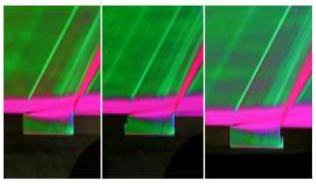

Figure 31. Re = 7 x10^6. (a) Straight edge cavity. (b) 120^0 leading edge serrations. (c) 120^0 trailing edge serrations.

The third image does not show any large differences to the straight edge situation. However, it is also quite noticeable that the expansion fan at the trailing edge is spread out over the serration showing up as a wider region than in the straight edge case.

2. High Speed Images

Analysis of single schlieren images indicates that the effect addition of serrations is more prominent for the 60 degree serrations. Therefore, only 60 degree serrations were investigated using time resolved schlierenVisualisation and unsteady pressure measurements.

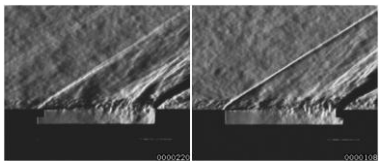

Figure 33. Re = 7.2 x 106. (a) At 60^0 leading edge serration. (b) At 60^0 trailing edge serration.

Weaker leading edge shock.The noticeable difference in the time resolved images is that by addition of serrations to leading edge, the leading edge shock has weakened. This occurs because the shock generating edge is discontinuous instead of straight. However, the thickness of the shear layer seems to have increased slightly as seen in figure.

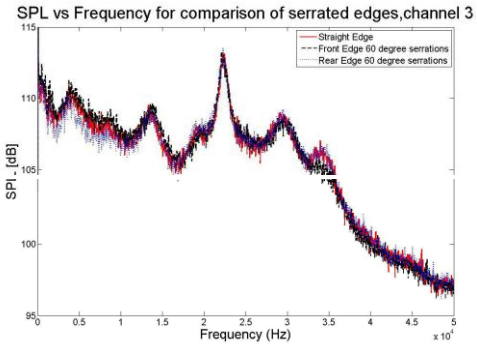

Figure 34. Effect of serrations on the sound pressure level within an simple open cavity.

To confirm these results, the overall sound pressure level was calculated and plotted against the pressure transducer location within the cavity. The equation that was used to plot the graph used the following definition for SPL:

$$OASPL = 20\log_{10}\left(\frac{P_{rms}}{P_r}\right)$$

Figure 35 shows that the overall sound pressure level does not vary much with the different transducer locations within the cavity. Of note is the addition of serrations, which have no significant effect on the OASPL either. The OASPLs shown in the above plot are higher than those that are considered in previous plots as it takes into account the power associated with the combined frequencies.

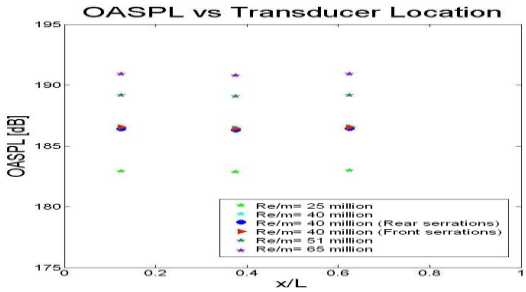

Figure 35. Overall sound pressure level versus transducer location.

Hybrid Mesh for Simple Cavity

Now hybrid meshing is carried out for the cavity structure,which shown as below.

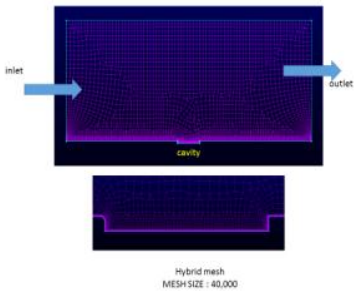

Fig 36 hybrid meshing

ANSYS ANLAYSIS

Now ansys analysis is carried out for all different cavities with help of ANSYS software.

STATIC PRESSURE CONTOUR

Static Pressure Contour In Simple Cavity

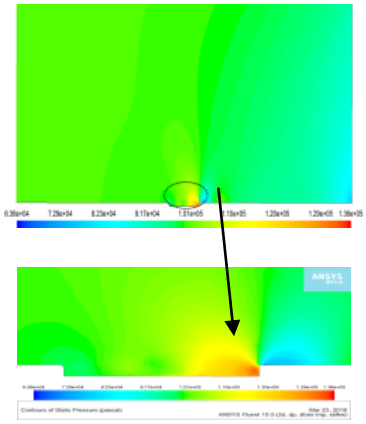

Static Pressure Distribution Of Vent Cavity

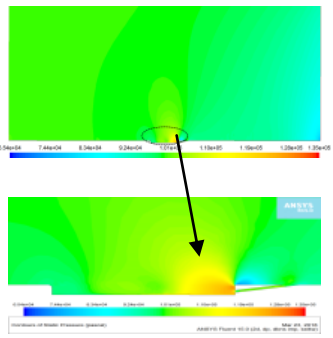

Solutions from Structural mechanics ANSYS provide the capability to replicate each structural aspect of a product, along non-linear static analysis so as to provides stresses & deformations, the modal analysis that determines vibration characteristics, through to superior transient nonlinear phenomena involving dynamic effects & complex behavior material.

Acoustic power level analysis

In acoustic power lavel analysis we carried out ANSYS analysis for acoustic power level in different types of cavities when cavity incounter incoming wind.

1. **Acoustic power level in simple cavity**

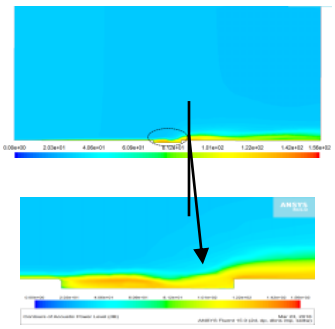

2. **Acoustic power level in vent cavity**

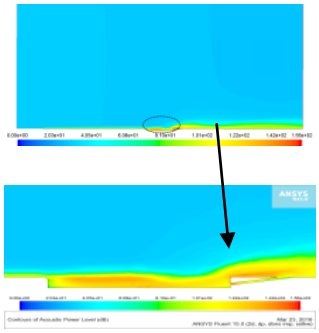

Comparison between static pressure distribution

Now comparison carried out for static pressure distribution for different types of cavities with the help of ANSYS software .in this I got the result that static pressure distribution is uniform in cavity with passive venting.

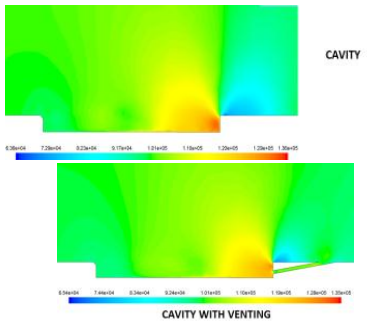

Fig 37 Comparison between static pressure distribution

Comparison between acoustic power level contour

Now comparison carried out for acoustic power level contour for different types of cavities with the help of ANSYS software . the result I got from this comparison is that the acoustic power level counter is low in case of passive venting cavity as compared to other cavities.

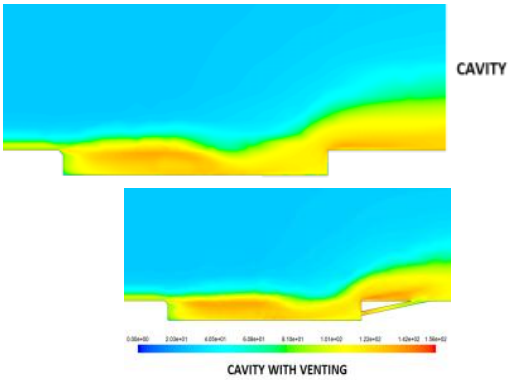

Fig 38 Comparison between acoustic power level contour

V. CONCLUSION

The experiments conducted have confirmed previous results concerning flow over shallow straight cavities. The sound pressure levels within the cavities are consistent with previous experiments and the measured frequencies are approximately in agreement with the Rossiter frequencies. The time resolved schlieren visualisation enabled the calculation of the fundamental frequency by directly tracking the path of individual waves and this frequency was in reasonable agreement with the calculated value. It is believed this is the first time that this direct verification has been carried out.

A linear relationship is shown to exist between root mean square cavity pressure and Reynolds number. The e addition or serrations had no significant effect on the flow. There was no evidence to suggest that serrated edge, whether they are leading or trailing edge serrations, were able to change the sound pressure levels or the presence of discrete frequencies.

Now in the case of venting the cavity as confirm from static pressure distribution analysis that the pressure distribution is uniform in the case of vent cavity as compare to the simple cavity. And from sound pressure level comparison its comes that there are a OASPL change in lower of vent cavity compare to simple cavity.

VI. RECOMMENDATIONS

The research into passive control of supersonic cavity flow should be continued. It is recommended that further research be conducted into serrations and vent cavity . Their configuration should be altered so that they act more like spoiler gates and protrude vertically into the flow.

Further research should be conducted into pressure sensitive paints. This particular measurement technique has a lot of potential for use with unsteady flows and with a new top window for the wind tunnel there is more scope for this area of research.

REFERENCES

[1] R.L. Stallings Jr. Store Separation from Cavities at Supersonic Flight Speeds. Journal of Spacecraft and Rockets,20(2):129{132, March-April 1983.

[2] A.B. Blair Jr and R.L. Stallings Jr. Cavity Door Ejects on Aerodynamic Loads of Stores Separating fromCavities. Journal of Aircraft, 26(7):615{620, July 1989J.

[3] J.E. Rossiter. Wind Tunnel Experiments on the Flow Over Rectangular Cavities at Subsonic and TransonicSpeeds. Technical Report 64037, Royal Aircraft Establishment, October 1964..

[4] F.J. Wilcox Jr. Experimental Measurements of Internal Store Separatio Characteristics at Supersonic Speeds.NASA Technical Report.

[5] D.P. Rizzetta and M.R. Visbal. Large-Eddy Simulation of Supersonic Cavity Flow_elds Including Flow Control. AIAAAIAA, 41(8):1438{1443, August 2003

[6] J.A. Ross and J.W. Peto. The E_ect of Cavity Shaping, Front Spoilers and Ceiling Bleed on Loads Acting on

[7] Passive control of super-sonic flow over cavity,Sally J Moon outh wales,thesis report 2008,UNSW@2008.

[8] L. Cattafesta, D. Williams, C. Rowley and F. Alvi. Review of Active Control of Flow-Induced Cavity Resonance.In 33rd AIAA Fluid Dynamics Conference. AIAA, June 2003. AIAA Paper 2003-3567.

[9] K.J. Badcock, B.E. Richards and M.A. Woodgate. Elements of Computational Fluid Dynamics on Block Structured Grids Using Implicit Solvers. Progress in Aerospace Sciences, 36:351{392, 2000.

[10] J.A. Ross. PIV Measurements of the Flow_elds in an Aerodynamically Deep Cavity, May 2002. Private Communication.

[11] Crawford R.J., "Supersonic cavity flows." School of Aerospace, Civil and Mechanical EngineerinG Canberra, University of New South Wales, B.E. (Aero), 1999.

[12] Crocco L. and Lees L., "A mixing Theory for the Interaction Between Dissipative Flows and Nearly Isentropic Streams." Journal of the Aeronautical Sciences, Vol. 19, No. 10, 1952, pp. 649-676.